analytical chemistry

Article

Cite This: *Anal. Chem.* 2018, 90, 11696−11702

pubs.acs.org/ac

Nanozyme Sensor Arrays for Detecting Versatile Analytes from Small Molecules to Proteins and Cells

Xiaoyu Wang,[†,§] Li Qin,[†,§] Min Zhou,[†] Zhangping Lou,[†] and Hui Wei*[,†,‡]

[†]Department of Biomedical Engineering, College of Engineering and Applied Sciences, Nanjing National Laboratory of Microstructures, Nanjing University, Nanjing, Jiangsu 210093, China

[‡]State Key Laboratory of Analytical Chemistry for Life Science and State Key Laboratory of Coordination Chemistry, School of Chemistry and Chemical Engineering, Collaborative Innovation Center of Chemistry for Life Sciences, Nanjing University, Nanjing, Jiangsu 210023, China

Supporting Information

ABSTRACT: Nanozymes have emerged as promising alternatives to overcome the high cost and low stability of natural enzymes. Nanozymes with peroxidase-like activities have been studied to construct versatile biosensors by using specific biorecognition ligands (such as enzymes, antibodies, and aptamers) or molecularly imprinted polymers (MIPs). However, the use of bioligands compromises the high stability and low cost promise of nanozymes, while the MIPs may not be applicable to multiplex detection. To address these limitations, here we constructed the nanozyme sensor arrays based on peroxidase-like Pt, Ru, and Ir nanozymes. The cross-reactive nanozyme sensor arrays were successfully used for the detection of biothiols and proteins as well as the discrimination of cancer cells because of the differential nonspecific interactions between the components of the sensor arrays and the analytes. The usefulness of the nanozyme sensor arrays was further validated by the detection of blind unknown samples, where 28 of 30 biothiols and 42 of 45 proteins were correctly identified. Moreover, the practical application of the nanozyme sensor arrays was demonstrated by the successful discrimination of biothiols in serum and proteins in human urine.

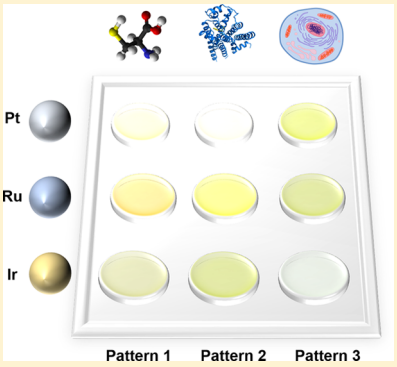

Catalytic nanomaterials with enzymatic activities (i.e., "nanozymes") have recently been developed to mitigate the natural enzymes' intrinsic limitations such as low stability and high cost.[1−3] Due to their tunable catalytic activities and multifunctionalities, nanozymes have been used for broad applications, ranging from biomedical detection[4−7] and therapy[8−12] to environmental protection[13] and national security.[14] Particularly, peroxidase-like nanozymes have been extensively studied to construct versatile biosensors.[2,4,15−17] For example, a selective glucose sensing strategy was developed by combining glucose oxidase with peroxidase-like Fe_3O_4 nanozymes.[5] The strategy has then been generalized to other analytes using the corresponding oxidases.[2,4] However, such a strategy is only applicable to the H_2O_2-producing analytes. On the other hand, when a specific biorecognition ligand (e.g., an antibody or an aptamer) is conjugated onto a peroxidase-like nanozyme, the conjugate can be used to develop highly selective sandwich and other related bioassays.[1,18] For instance, Yan's group reported two Fe_3O_4 nanozymes based immunoassays for disease biomarkers.[1] Despite the substantial success, the current nanozyme biosensors are generally based on the preselected bioligands (e.g., an oxidase or an antibody) for specific recognition, which may not be available for the emerging analytes. The use of bioligands also compromises the high stability and low cost promise of nanozymes. To address these concerns, Liu and co-workers recently developed substrate-specific nanozymes by growing molecularly imprinted polymers (MIPs) onto the nanozymes.[19,20] Like an antibody, however, each imprinted nanozyme has to be tailored to a given analyte. For certain delicate proteins, the imprinted nanozymes may not be applicable owing to the polymerization conditions. It is also challenging to perform multiplex detection with the imprinted nanozymes. To develop a universal nanozyme sensor with multiplex detection capacity, herein we use peroxidase-like nanozymes to construct cross-reactive sensor arrays for detecting analytes from bioactive small molecules to proteins and even cells (Scheme 1). As shown in Scheme 1, the nonspecific interactions between the components of the sensor arrays and analytes distinctly affect the nanozymes' catalytic reaction, enabling the sensor arrays to discriminate versatile analytes.

Inspired by the response of gustatory and olfactory systems to taste and smell, cross-reactive sensor arrays (the so-called artificial "noses/tongues") have been developed as promising alternatives to the traditional "one-to-one" biosensors.[21−24] They detect diverse analytes (such as metal ions,[25] small molecules,[26−28] biomacromolecules,[22,29−32] cells,[33,34] and bacteria[35,36]) by generating unique identification patterns,

Received: July 28, 2018
Accepted: September 3, 2018
Published: September 3, 2018

DOI: 10.1021/acs.analchem.8b03374
Anal. Chem. 2018, 90, 11696−11702

Scheme 1. Nanozyme Sensor Arrays for Detecting Versatile Analytes[a]

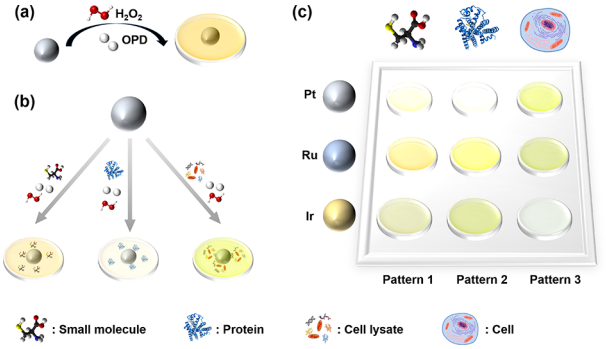

[a](a) Catalytic oxidation of *o*-phenylenediamine (OPD) in the presence of peroxidase-like nanozymes. (b) Catalytic oxidation of OPD in the presence of nanozyme with small molecules, proteins, and cells. (c) Pattern-based recognition of small molecules, proteins, and cells by Pt, Ru, and Ir nanozymes-based cross-reactive sensor arrays.

which are then analyzed using linear discriminant analysis (LDA) or other multivariate statistical methods. The cross-reactive sensor arrays are traditionally built with fluorescent dyes,[23] whose synthesis is tedious and fluorescence can be photobleached. Recently, nanomaterials have been used to construct sensor arrays, which are not only more cost-effective and robust but also easier to be synthesized and modulated.[26,27,32] Very recently, we reported the two-dimensional metal−organic framework (2D-MOF) nanozyme sensor arrays for probing phosphates and monitoring their enzymatic hydrolysis.[37] However, the detection of versatile analytes from bioactive small molecules to proteins and cells has not been demonstrated yet with nanozyme sensor arrays, which, if achieved, would represent a major step toward nanozyme bioanalysis. To fill this gap, herein we used peroxidase-like Pd, Ru, and Ir nanozymes to construct cross-reactive sensor arrays for versatile analytes. Using the sensor arrays, six biothiols, nine proteins, and five cancer cells were successfully discriminated. Moreover, the practical applications of the sensor arrays have been validated by the successful identification of unknown samples and by the discrimination of biothiols in serum and proteins in human urine.

EXPERIMENTAL SECTION

Chemicals and Materials. Chloroplatinic acid ($H_2PtCl_6·6H_2O$), sodium borohydride ($NaBH_4$), and lysozyme were obtained from Sigma-Aldrich. Ruthenium chloride hydrate ($RuCl_3·xH_2O$), iridium chloride hydrate ($IrCl_3·xH_2O$), poly(vinylpyrrolidone) (PVP, M_w 58 000), mercaptoacetic acid, L-cysteine (Cys), mercaptosuccinic acid, dithiothreitol, α-amylase, bovine serum albumin, trypsin, cytochrome *c* (cyt *c*), transferrin, and glucose oxidase were purchased from Aladdin Chemical Reagent Co., Ltd. Ethylene glycol, acetone, and hemoglobin were purchased from Sinopharm Chemical Reagent Co., Ltd. Glutathione (GSH) and mercaptoethanol were obtained from J&K Scientific. Human serum albumin (HSA) was obtained from CSL Behring AG (Switzerland). All aqueous solutions used in the experiments were prepared with deionized water (18.2 MΩ·cm, Millipore).

Instrumentation. Transmission electron microscopy (TEM) images were recorded on a JEOL JEM-2100 transmission electron microscope at an acceleration voltage of 200 kV. UV−vis absorption spectra were collected using a spectrophotometer (Cary-100, Agilent Technologies). The absorption of the 96-well plate at 450 nm was recorded by a microplate reader (RT-6000, Rayto Life and Analytical Sciences Co., Ltd.). X-ray photoelectron spectroscopy (XPS) was collected using a PHI 5000 VersaProbe (Ulvac-Phi, Japan). All the measurements were carried out with reference to C 1s binding energy (285 eV) as the internal standard. The ζ-potential distribution was measured on a Nanosizer ZS90 (Malvern).

Synthesis of Pt Nanozymes. The Pt nanozymes were synthesized as follows.[38] Briefly, aqueous solutions of H_2PtCl_6 (1 mL, 16 mM) and trisodium citrate (1 mL, 40 mM) were added into 38 mL of water and stirred for 30 min under room temperature. Then, $NaBH_4$ (200 μL, 50 mM) was added dropwise into the mixture. The mixture was reacted and stirred for 1 h at room temperature.

Synthesis of Ru and Ir Nanozymes. Ru or Ir nanozymes were synthesized as follows.[39] Briefly, 0.1 mmol of $RuCl_3·xH_2O$ (or 0.1 mmol $IrCl_3·xH_2O$), 100 mg of PVP (k-30), and 10 mL of ethylene glycol were mixed in a flask. The mixture was heated up to 120 °C and kept at this temperature for 20 min under continuous stirring. Then, the mixture solution was heated up to 195 °C and kept for 1 h. After cooling down, Ru (or Ir) nanoparticles were obtained by washing the resulting reaction solution with ethanol and acetone.

Effect of Biothiols on Nanozyme Activity. To verify the feasibility for biothiols discrimination, we first measured the effect of different biothiols on nanozymes' activities. At the optimum pH, the mixtures of 5 μg of Pt, 8 μg of Ru, or 2 μg of Ir nanozymes and different concentrations of biothiols were incubated for 20 min. Then, 50 μL of H_2O_2 (200 mM) and 50 μL of *o*-phenylenediamine (OPD) (40 mM) with NaOAc buffer (0.2 M, pH 4.5) were added to a final volume of 1 mL. The reaction solution was maintained in a 37 °C water bath for 20 min. Then, the absorption spectra were measured.

Biothiols Discrimination. Biothiols were detected as follows. To each nanozyme, a 7 × 5 region in a 96-well plate was selected where the blank and six biothiols occupied a 5-well line, respectively. An amount of 80 μL of buffer solution (0.2 M NaOAc, pH 4.5) was added into each well, including appropriate amounts of biothiols and nanozymes. After incubation for 20 min at room temperature, 10 μL of H_2O_2 (100 mM) and 10 μL of OPD (20 mM) were rapidly added into each well to a final volume of 100 μL. Immediately after the addition of chromogenic substrate, the absorption of each sample at 450 nm was recorded by a microplate reader at an interval of 5 min for 20 min. The concentrations of Pt, Ru, and Ir nanoparticles (NPs) were 5, 8, and 2 μg/mL, respectively. Thus, the six biothiols were tested against the three nanozymes five times to give a six thiols × three arrays × five replicates training data matrix. The raw data matrix was processed using LDA.

Biothiols-spiked fetal bovine serum (FBS) was taken as an example to test the practical application of the as-prepared sensor arrays for real samples.

Proteins Discrimination. Proteins were detected as follows. First, 40 μL of protein solution with a certain concentration was mixed with the nanozyme solution and kept for 60 min incubation. The total volume of the mixed solution was 200 μL. The concentrations of Pt, Ru, and Ir nanozymes were 10, 10, and 5 μg/mL, respectively. Then, 10 μL of the incubated solution, 70 μL of NaOAc buffer (0.2 M, pH 4.5),

DOI: 10.1021/acs.analchem.8b03374
Anal. Chem. 2018, 90, 11696−11702

10 μL of H_2O_2 (400 mM), and 10 μL of OPD (20 mM) were added into each well of a 96-well plate subsequently. Immediately after the addition of OPD, the absorption of each sample at 450 nm was recorded by a microplate reader at an interval of 10 min for 40 min.

Urine sample was collected and centrifuged for 10 min under 10 000 rpm to remove insoluble matrix. Urine diluted 50-fold was used for proteins discrimination to test the practical application of the sensor arrays for a real sample of proteins.

Kinetics Assays. All steady-state kinetics assays were conducted at room temperature in 1.0 mL cuvettes with a path length of 1.0 cm. A 0.2 M NaOAc buffer solution (pH 4.5) was used as the reaction buffer. Final concentrations of 10, 5, and 1 μg/mL of Pt, Ru, and Ir nanozymes were used for their kinetics assays. The kinetics measurements of Ir−GSH, Ir−Cys, and Ir−HSA were carried out after incubating the Ir nanoparticles with GSH, Cys, and HSA for 30 min. The final concentration of Ir nanoparticles for kinetics assays of Ir−GSH, Ir−Cys, and Ir−HSA was 1 μg/mL, while the final concentrations of GSH, Cys, and HSA were 10, 10, and 1 μM. The kinetics data were obtained by varying the concentration of one substrate of H_2O_2 or 3,3′,5,5′-tetramethylbenzidine (TMB) while keeping the other's concentration constant. In the suitable concentration range of H_2O_2 and TMB, typical Michaelis−Menten curves were obtained.

Cell Culture and Lysate Preparation. Cells were cultured in high-glucose Dulbecco's modified Eagle's medium (DMEM) culture medium supplemented with 10% FBS and 1% penicillin−streptomycin (10 000 U/mL) under the atmosphere of 5% CO_2 at 37 °C. When the cell density reached 80%, 10^8 cells were collected and washed with precold phosphate-buffered saline (PBS) three times, and then the cells precipitations were suspended in 200 μL of precold lysis buffer [0.15 mM NaCl, 5 mM EDTA, 1% Triton-X 100, 10 mM Tris−HCl (pH 7.4) with appropriate protease inhibitor]. These cells were disrupted by ultrasonication for 1 min under low power, and all processes were operated in low temperature. Then, the cell lysate was centrifuged at 4 °C for 10 min at 13 000 rpm. The supernatants were transferred to sterile tubes for the following discrimination assays.

Cell Discrimination. Cells were detected as follows. All the cell lysate solutions were diluted at the same cell concentration (85 000/mL). First, 10 μL of cell lysate solutions were mixed with the appropriate concentration of each nanozyme and incubated for 20 min. The total volume of mixed solution was 200 μL, and the concentrations of Pt, Ru, Ir nanozymes were 10, 10, and 2.5 μg/mL, respectively. Then, 10 μL of the incubated solution, 70 μL of NaOAc buffer (0.2 M, pH 4.5), 10 μL of H_2O_2 (400 mM), and 10 μL of OPD (20 mM) were added into each well of a 96-well plate subsequently. Then, the absorption of each sample at 450 nm was recorded by a microplate reader at an interval of 10 min for 40 min.

RESULTS AND DISCUSSION

Synthesis and Characterization of Pt, Ru, and Ir Nanozymes. The formation of Pt, Ru, and Ir nanozymes was first confirmed by TEM imaging and XPS spectra (Figure 1a−c and Figures S1 and S2). As shown in Figure 1a−c and Figure S1, the Pt, Ru, and Ir NPs were roughly spherical with average sizes of 3.5, 2, and 1.8 nm, respectively. More, the high-resolution TEM image in Figure S1b indicated the continuous lattice spacing of 0.223 nm corresponding to the (111) facet of the face-centered cubic (fcc) Pt NPs. The distances of the adjacent fringes of 0.221 and 0.205 nm in Figure S1d−f were assigned to the lattice spacing of the (101) and (111) facets of Ru and Ir NPs, respectively. XPS measurements were performed to characterize the chemical states and surface properties of as-synthesized Pt, Ru, and Ir NPs (Figure S2). The Pt $4f_{7/2}$ of Pt NPs was deconvoluted into two distinct components, which were assigned to Pt^0 and Pt^{2+}, with binding energy at 71.14 and 72.40 eV, respectively. The Ru $3p_{3/2}$ of Ru NPs was deconvoluted into two peaks, which belonged to Ru^0 and Ru^{4+}, respectively. The Ir $4f_{7/2}$ of Ir NPs was deconvoluted into two distinct components assigned to Ir^0 and $Ir^{\delta+}$, with binding energy at 60.80 and 61.53 eV, respectively.

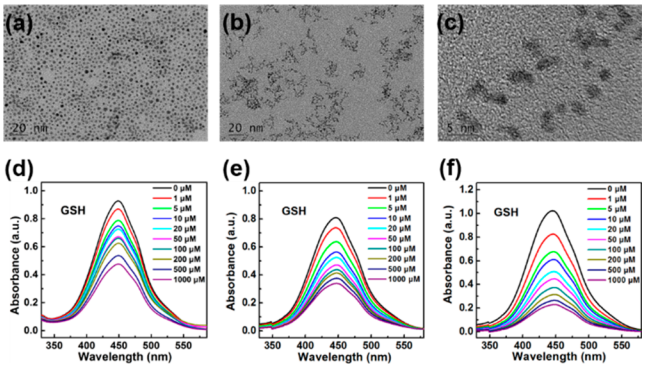

Figure 1. (a−c) Representative TEM images of Pt, Ru, and Ir nanozymes. Typical absorption spectra for monitoring the catalytic oxidation of OPD in the presence of (d) Pt, (e) Ru, and (f) Ir nanozymes with various concentrations of GSH.

After successful synthesis of Pt, Ru, and Ir nanozymes, their peroxidase-like activity was evaluated by monitoring the catalytic oxidation of OPD with H_2O_2. The catalytic oxidation of OPD generated the oxidized product with a characteristic absorption peak at around 450 nm. As shown in Figure S4a−c, OPD with the three nanozymes (Pt, Ru, or Ir) and H_2O_2 incubated at 37 °C for 10 min showed strong absorption values at 450 nm. The control experiments suggested that the solutions contained OPD alone, H_2O_2 and OPD, or nanozymes and OPD showed negligible color changes. Moreover, all the three peroxidase substrates, i.e., TMB, 2,2′-azino-bis(3-ethylbenzothiazoline-6-sulfonic acid) diammonium (ABTS), and OPD, showed strong absorbance due to the catalytic oxidation with Pt, Ru, and Ir nanozymes in the presence of H_2O_2 (Figure S4d−f). Similar with natural enzymes, Pt, Ru, and Ir nanozymes showed H_2O_2 concentrations, catalyst concentrations, and pH-dependent peroxidase-like activity (Figure S5). The steady-state kinetics assays of Pt, Ru, and Ir nanozymes were conducted (Figures S6−S8). The kinetics data of three nanozymes and horseradish peroxidase (HRP) are listed in Table S1. As seen in Table S1, these nanozymes showed high V_{max} values for both H_2O_2 and TMB, suggesting that these nanozymes can efficiently catalyze the oxidation of peroxidase substrates. The above results demonstrated that Pt, Ru, and Ir nanozymes exhibited excellent peroxidase-like activity.

Nanozyme Sensor Arrays for Biothiols. They were then used to construct the nanozyme sensor arrays. To demonstrate the feasibility of the sensor arrays, the discrimination of biothiols was first performed. As a model of bioactive small molecules, biothiols, such as Cys and GSH, play crucial roles in various physiological and pathological processes.[40,41] The

DOI: 10.1021/acs.analchem.8b03374
Anal. Chem. 2018, 90, 11696−11702

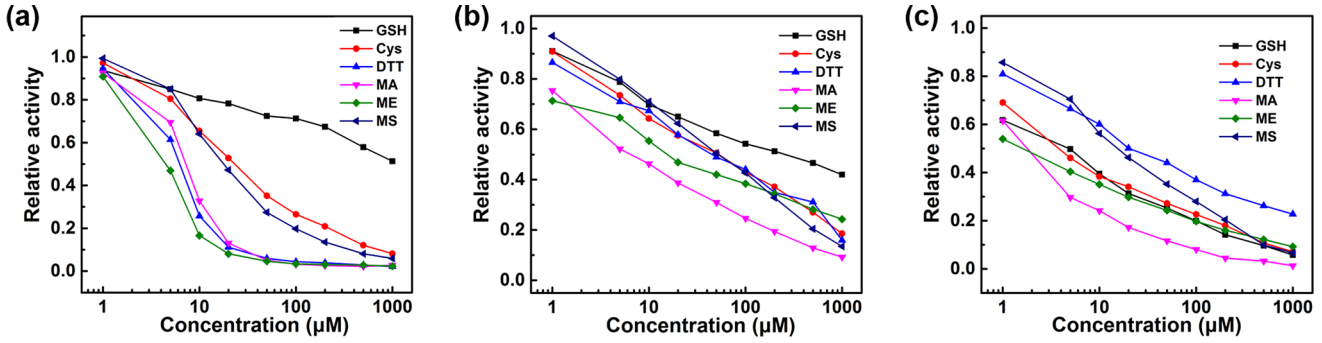

Figure 2. Normalized peroxidase-mimicking activity of (a) Pt, (b) Ru, and (c) Ir nanozymes after incubation with different concentrations of the six biothiols.

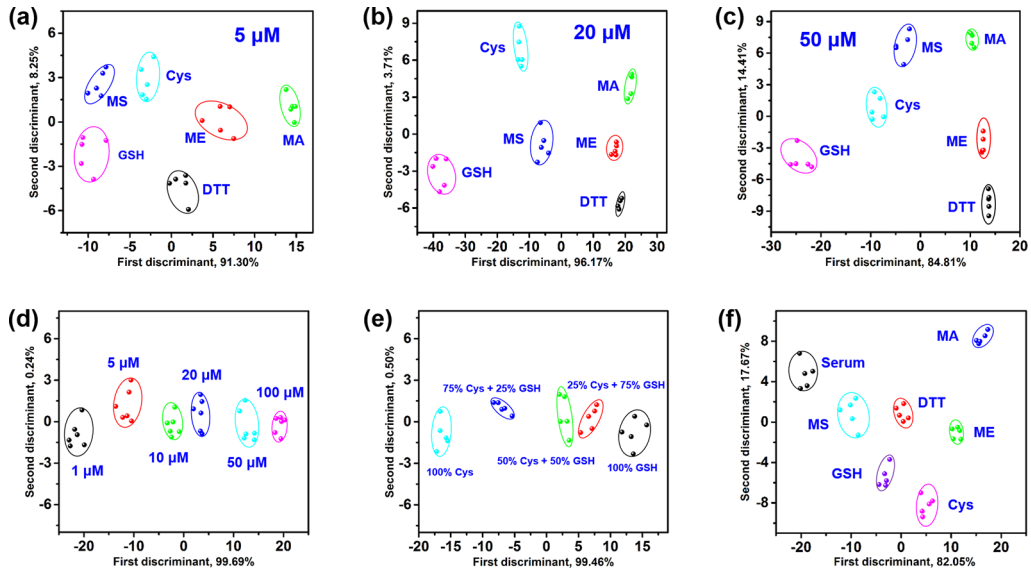

Figure 3. Nanozyme sensor arrays for biothiols. Two-dimensional canonical score plots for the first two factors of response patterns obtained against (a) 5 μM, (b) 20 μM, and (c) 50 μM of biothiols. Two-dimensional canonical score plots for the first two factors of response patterns obtained against six different concentrations of Cys (d), the mixtures of Cys and GSH at different molar ratios (total concentration at 20 μM) (e), and 10 μM of biothiols in the presence of 1% FBS (f). The canonical scores were calculated by LDA for the identification and discrimination of biothiols.

abnormal level of biothiols correlates with various diseases including cancer, liver damage, psoriasis, etc.[40,41] Though biothiols have been determined with nanozymes, the previous competitive methods were not able to differentiate biothiols from each other since a single nanozyme was not specific for biothiols.[42] Here, a sensor array was therefore constructed with the Pt, Ru, and Ir nanozymes to detect and discriminate various biothiols. Six typical biothiols including GSH, Cys, mercaptoacetic acid (MA), mercaptosuccinic acid (MS), dithiothreitol (DTT), and mercaptoethanol (ME) were selected as analytes to evaluate the sensor arrays (Figure S9).

Since the sensing principle of the sensor array for biothiols was based on their differential competitive effects on the activity of nanozymes, we first studied the peroxidase-like activities of Pt, Ru, and Ir nanozymes in the presence of biothiols. As shown in Figure 1d–f, the absorption of oxidized OPD (oxOPD) decreased as the concentration of GSH increased, suggesting that GSH showed the competitive effect on the catalytic activity of Pt, Ru, and Ir nanozymes. Moreover, the six biothiols exhibited obviously different competitive effects on the same nanozyme and each biothiol also showed different competitive effects on different nanozymes (Figure 2 and Figures S10–S12), indicating the feasibility of biothiol discrimination using such sensor arrays.

To test the discrimination capability of the sensor arrays, the responses of the nanozymes to various biothiols were studied first. The relative change of absorption of oxOPD [i.e., $(A_0 - A)/A_0$, where A and A_0 were the absorption of oxOPD at 450 nm in the presence and absence of analytes in the nanozyme reaction systems, respectively] was used to construct the colorimetric response patterns (or "fingerprint maps") for 5 μM of biothiols (Figure S13). Then, the response patterns were subjected to LDA analysis to convert the training matrix into three canonical scores, and the first two most important discrimination factors were used to generate 2D canonical score plots. As shown in Figure 3a, the canonical patterns were clustered into six groups, and all the biothiols were separated entirely from each other with no errors or misclassifications. To further evaluate the discrimination power of the sensor arrays for biothiols, other sets of concentrations (10, 20, 50, and 100 μM) were tested (Figure 3, parts b and c, and Figures S14 and S15). Similar to the concentration of 5 μM, the biothiols at each concentration produced specific response patterns and were clustered into six different groups. These

DOI: 10.1021/acs.analchem.8b03374
Anal. Chem. 2018, 90, 11696–11702

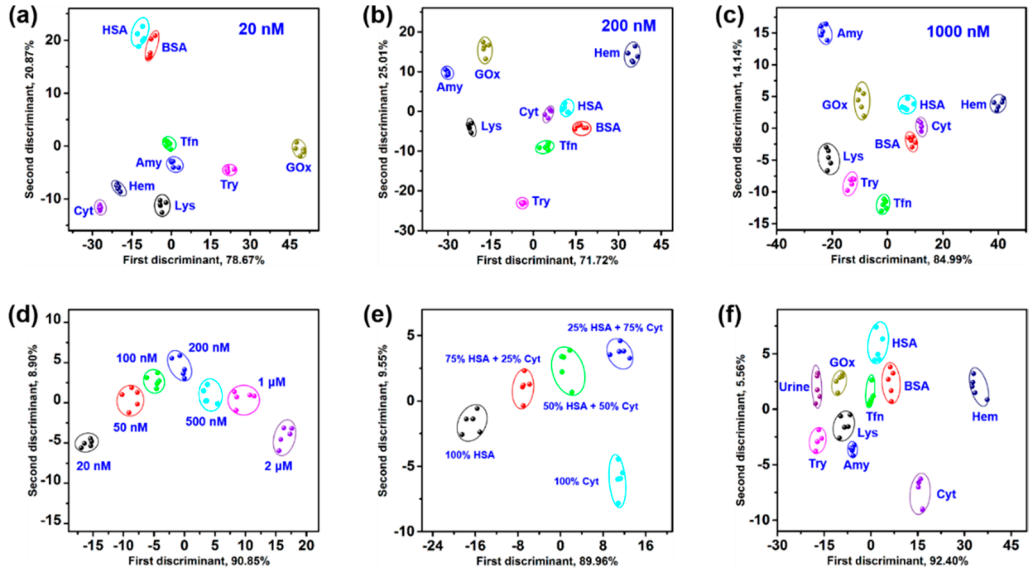

Figure 4. Nanozyme sensor arrays for proteins. Two-dimensional canonical score plots for the first two factors of response patterns obtained against (a) 20 nM, (b) 200 nM, and (c) 1 μM of various proteins. Two-dimensional canonical score plots for the first two factors of response patterns obtained against seven different concentrations of HSA (d), the mixtures of HSA and cyt *c* (labeled as Cyt) at different molar ratios (total concentration at 1 μM) (e), and 200 nM of proteins in the presence of human urine (f). The canonical scores were calculated by LDA for the identification of proteins.

results clearly demonstrated that the sensor arrays had good differentiation capability for biothiols in broad concentration ranges.

To illustrate the quantitative capability of the sensor arrays, the discrimination assays of Cys with various concentrations were conducted as an example. As shown in Figure 3d, Cys at concentrations varying from 1 to 100 μM were well-discriminated. Moreover, a quantitative response curve for Cys was obtained by plotting the canonical variable 1 against the concentration of Cys (Figure S16).

To examine the multiplex detection ability of the sensor arrays, the discrimination of the mixtures of GSH and Cys with different ratios was performed. As shown in Figure 3e, these mixtures with different molar ratios were clustered into different groups and all groups were separated from each other, demonstrating the multiplex discrimination capability of the sensor arrays.

Then, the discrimination of biothiols in fetal bovine serum (FBS) was taken as an example to demonstrate the practical application of the sensor arrays. The response patterns of serum in the absence and presence of 100 μM of biothiols were measured, and the response patterns were subsequently subjected to LDA. As shown in Figure S17, the sensor arrays performed well for discrimination of the six biothiols in serum. Moreover, the biothiols with even lower concentrations of 10 and 20 μM in serum were discriminated after suitable sample pretreatment (Figure 3f and Figure S18).

An ultimate test of the practical applications of the sensor arrays is to identify unknown samples. The identification of unknown biothiols was based on the above training sets. The response patterns of 30 unknown biothiols were obtained by the same LDA clustering approach. The Mahalanobis squared distances between the unknown samples and each training biothiol group were determined by LDA. The minimal Mahalanobis square distance indicated the sample belonged to the corresponding biothiol group. Using this method, 28 of 30 unknown biothiols were correctly identified with a 93.3% identification accuracy (Table S2). The above results suggested the potential applications of the sensor arrays for discriminating biothiols in real samples.

Nanozyme Sensor Arrays for Proteins. Having demonstrated the discrimination capability of the sensor arrays toward bioactive small molecules (i.e., biothiols), we further tested their discrimination ability for proteins. Nine typical proteins with different characteristics were chosen for analysis (Table S3). First, we recorded the kinetic curves of A_{450} of oxOPD in the absence and presence of various proteins. As shown in Figure S19, differentiable kinetic curves were obtained after adding the nine proteins into the nanozyme catalytic reaction systems. Differential interactions between the nine proteins and nanozyme made it possible to discriminate proteins using nanozyme sensor arrays.

Then, the response patterns were generated by collecting the A/A_0 values at the concentration of 20 nM of all nine proteins (Figure S21), which suggested that the change profiles of absorption had a unique fingerprint for each protein. After the LDA, the response patterns of 20 nM of proteins against the sensor arrays were clustered to nine distinct groups with no overlap (Figure 4a), suggesting the successful discrimination of the nine proteins with an identification accuracy of 100%. To further verify the broad sensing range of the sensor arrays, we tested the proteins at the concentrations of 50, 100, and 200 nM and 1 and 2 μM, respectively (Figure 4, parts b and c, and Figures S22–S24). All the concentrations were successfully clustered to nine distinct groups with no overlap.

After successful discrimination of nine proteins with a given concentration, the next challenges are to quantitatively determine the concentration of a given protein and to perform multiplex detection. The quantitative assays of HSA and cyt *c* were taken as examples. As shown in Figure 4d and Figure S26b, the LDA plots for HSA and cyt *c* with various concentrations were clustered into distinct groups with no errors or misclassifications, demonstrating the quantitative power of the sensor arrays. The quantitative response curves

DOI: 10.1021/acs.analchem.8b03374
Anal. Chem. 2018, 90, 11696−11702

were also obtained between the concentration of proteins and the values of canonical variable 1 (Figures S25 and S26c), enabling the protein quantitation. Moreover, the response patterns of the mixtures of HSA and cyt *c* with various molar ratios were obtained. As shown in Figure 4e, five groups of protein mixtures were clustered to five independent groups without overlap, suggesting the multiplex discrimination capability of the sensor arrays toward proteins.

To test the practical application of the sensing arrays toward proteins, the protein-spiked biofluids and the unknown protein samples were further evaluated. The response patterns were obtained by applying the human urine samples spiked with the nine proteins to the sensor arrays. As shown in Figure 4f and Figure S27, proteins at the concentrations of 200 and 500 nM were clearly differentiated with no errors. Moreover, for 45 unknown protein samples, 42 were correctly classified with an identification accuracy of 93.3% (Table S5). These results validated the great promise of the sensor arrays for identifying proteins in real biological samples with complex matrix.

Nanozyme Sensor Arrays for Cells. Finally, to further validate the universality and discrimination power of the sensor arrays, we elaborated our sensor arrays to identify cancer cells with various tissue origins, including A2780, Hep-G2, MCF-7, Hela, and 4T1 (Figure 5a). The normalized change of absorption values at 450 nm (A/A_0) was analyzed by LDA. As shown in Figure 5b, the response of A/A_0 was clearly clustered into five groups with no overlap, indicating the successful discrimination for five cancer cells using the sensor arrays.

(a)

#	Cell line	Tissue origin	Cell status
1	A2780	Ovarian	Cancerous
2	Hep-G2	Liver	Cancerous
3	MCF-7	Breast	Cancerous
4	Hela	Cervial	Cancerous
5	4T1	Breast	Cancerous

(b)

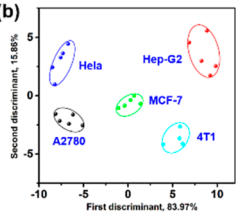

Figure 5. Nanozyme sensor arrays for cells. (a) Features of five cancerous cell lines with different tissue origins. (b) Two-dimensional canonical score plot for the first two factors of response patterns obtained against five cancerous cell lines. The canonical scores were calculated by LDA for the identification of five cancerous cell lines.

CONCLUSIONS

In summary, we have developed universal sensor arrays based on peroxidase-like Pt, Ru, and Ir nanozymes and demonstrated the utility in detecting and discriminating analytes from small molecules to proteins as well as cells. Using the sensor arrays, six biothiols, nine proteins, and five cancer cells were successfully discriminated. The utility of the sensor arrays was further validated by the successful identification of unknown samples. Moreover, the practical applications of the sensor arrays were demonstrated by the discrimination of biothiols in serum and proteins in human urine. This work not only addresses the current challenges of the nanozyme bioanalysis but also provides promising strategies for biomedical diagnostics. However, the current sensor arrays are not suitable for detecting specific groups of biomarkers in biofluids. To address the limitations of our system, nanozyme sensor arrays for analyzing specific biomarkers in biofluids should be developed in subsequent research.

ASSOCIATED CONTENT

Supporting Information

The Supporting Information is available free of charge on the ACS Publications website at DOI: 10.1021/acs.analchem.8b03374.

Characterization of nanoparticles and nanozymes, kinetics, colorimetric response patterns of the nanozyme sensor arrays, and identification of unknown biothiol and protein samples (PDF)

AUTHOR INFORMATION

Corresponding Author

*E-mail: weihui@nju.edu.cn. Fax: +86-25-83594648. Phone: +86-25-83593272.

ORCID

Xiaoyu Wang: 0000-0002-8641-2430

Hui Wei: 0000-0003-0870-7142

Author Contributions

The manuscript was written through contributions of all authors.

Author Contributions

§X.W. and L.Q. contributed equally to this work.

Notes

The authors declare no competing financial interest.

ACKNOWLEDGMENTS

This work was supported by the National Natural Science Foundation of China (21722503 and 21874067), the 973 Program (2015CB659400), the PAPD program, the Shuangchuang Program of Jiangsu Province, the Open Funds of the State Key Laboratory of Analytical Chemistry for Life Science (SKLACLS1704), the Open Funds of the State Key Laboratory of Coordination Chemistry (SKLCC1819), the Fundamental Research Funds for the Central Universities (021314380103), and the Thousand Talents Program for Young Researchers.

REFERENCES

(1) Gao, L.; Zhuang, J.; Nie, L.; Zhang, J.; Zhang, Y.; Gu, N.; Wang, T.; Feng, J.; Yang, D.; Perrett, S.; Yan, X. *Nat. Nanotechnol.* **2007**, *2*, 577−583.
(2) Wei, H.; Wang, E. *Chem. Soc. Rev.* **2013**, *42*, 6060−6093.
(3) Lin, Y.; Ren, J.; Qu, X. *Acc. Chem. Res.* **2014**, *47*, 1097−1105.
(4) Wang, X.; Hu, Y.; Wei, H. *Inorg. Chem. Front.* **2016**, *3*, 41−60.
(5) Wei, H.; Wang, E. *Anal. Chem.* **2008**, *80*, 2250−2254.
(6) Fan, K.; Cao, C.; Pan, Y.; Lu, D.; Yang, D.; Feng, J.; Song, L.; Liang, M.; Yan, X. *Nat. Nanotechnol.* **2012**, *7*, 459−464.
(7) Liu, B.; Liu, J. *Nano Res.* **2017**, *10*, 1125−1148.
(8) Huo, M.; Wang, L.; Chen, Y.; Shi, J. *Nat. Commun.* **2017**, *8*, 357.
(9) Singh, N.; Savanur, M. A.; Srivastava, S.; D'Silva, P.; Mugesh, G. *Angew. Chem., Int. Ed.* **2017**, *56*, 14267−14271.
(10) Kim, C. K.; Kim, T.; Choi, I.-Y.; Soh, M.; Kim, D.; Kim, Y.-J.; Jang, H.; Yang, H.-S.; Kim, J. Y.; Park, H.-K.; Park, S. P.; Park, S.; Yu, T.; Yoon, B.-W.; Lee, S.-H.; Hyeon, T. *Angew. Chem., Int. Ed.* **2012**, *51*, 11039−11043.
(11) Zhang, Y.; Wang, F.; Liu, C.; Wang, Z.; Kang, L.; Huang, Y.; Dong, K.; Ren, J.; Qu, X. *ACS Nano* **2018**, *12*, 651−661.
(12) Zhang, W.; Hu, S.; Yin, J.-J.; He, W.; Lu, W.; Ma, M.; Gu, N.; Zhang, Y. *J. Am. Chem. Soc.* **2016**, *138*, 5860−5865.
(13) Natalio, F.; Andre, R.; Hartog, A. F.; Stoll, B.; Jochum, K. P.; Wever, R.; Tremel, W. *Nat. Nanotechnol.* **2012**, *7*, 530−535.
(14) Vernekar, A. A.; Das, T.; Mugesh, G. *Angew. Chem., Int. Ed.* **2016**, *55*, 1412−1416.

DOI: 10.1021/acs.analchem.8b03374
Anal. Chem. 2018, 90, 11696−11702

(15) Wang, Q.; Zhang, X.; Huang, L.; Zhang, Z.; Dong, S. *Angew. Chem., Int. Ed.* **2017**, *56*, 16082−16085.
(16) Hu, Y.; Cheng, H.; Zhao, X.; Wu, J.; Muhammad, F.; Lin, S.; He, J.; Zhou, L.; Zhang, C.; Deng, Y.; Wang, P.; Zhou, Z.; Nie, S.; Wei, H. *ACS Nano* **2017**, *11*, 5558−5566.
(17) Pratsinis, A.; Kelesidis, G. A.; Zuercher, S.; Krumeich, F.; Bolisetty, S.; Mezzenga, R.; Leroux, J.-C.; Sotiriou, G. A. *ACS Nano* **2017**, *11*, 12210−12218.
(18) Ye, H.; Yang, K.; Tao, J.; Liu, Y.; Zhang, Q.; Habibi, S.; Nie, Z.; Xia, X. *ACS Nano* **2017**, *11*, 2052−2059.
(19) Zhang, Z.; Zhang, X.; Liu, B.; Liu, J. *J. Am. Chem. Soc.* **2017**, *139*, 5412−5419.
(20) Zhang, Z.; Liu, Y.; Zhang, X.; Liu, J. *Nano Lett.* **2017**, *17*, 7926−7931.
(21) Rakow, N. A.; Suslick, K. S. *Nature* **2000**, *406*, 710−713.
(22) You, C.-C.; Miranda, O. R.; Gider, B.; Ghosh, P. S.; Kim, I.-B.; Erdogan, B.; Krovi, S. A.; Bunz, U. H. F.; Rotello, V. M. *Nat. Nanotechnol.* **2007**, *2*, 318−323.
(23) Diehl, K. L.; Anslyn, E. V. *Chem. Soc. Rev.* **2013**, *42*, 8596−8611.
(24) Ko, J.; Bhagwat, N.; Yee, S. S.; Ortiz, N.; Sahmoud, A.; Black, T.; Aiello, N. M.; McKenzie, L.; O'Hara, M.; Redlinger, C.; Romeo, J.; Carpenter, E. L.; Stanger, B. Z.; Issadore, D. *ACS Nano* **2017**, *11*, 11182−11193.
(25) Liu, Y.; Mettry, M.; Gill, A. D.; Perez, L.; Zhong, W.; Hooley, R. J. *Anal. Chem.* **2017**, *89*, 11113−11121.
(26) Sun, S.; Jiang, K.; Qian, S.; Wang, Y.; Lin, H. *Anal. Chem.* **2017**, *89*, 5542−5548.
(27) Peng, G.; Tisch, U.; Adams, O.; Hakim, M.; Shehada, N.; Broza, Y. Y.; Billan, S.; Abdah-Bortnyak, R.; Kuten, A.; Haick, H. *Nat. Nanotechnol.* **2009**, *4*, 669−673.
(28) Zhang, W.; Gao, N.; Cui, J.; Wang, C.; Wang, S.; Zhang, G.; Dong, X.; Zhang, D.; Li, G. *Chem. Sci.* **2017**, *8*, 6281−6289.
(29) Lu, Y.; Liu, Y.; Zhang, S.; Wang, S.; Zhang, S.; Zhang, X. *Anal. Chem.* **2013**, *85*, 6571−6574.
(30) Pode, Z.; Peri-Naor, R.; Georgeson, J. M.; Ilani, T.; Kiss, V.; Unger, T.; Markus, B.; Barr, H. M.; Motiei, L.; Margulies, D. *Nat. Nanotechnol.* **2017**, *12*, 1161−1168.
(31) Motiei, L.; Pode, Z.; Koganitsky, A.; Margulies, D. *Angew. Chem., Int. Ed.* **2014**, *53*, 9289−9293.
(32) Li, X.; Wen, F.; Creran, B.; Jeong, Y.; Zhang, X.; Rotello, V. M. *Small* **2012**, *8*, 3589−3592.
(33) Rana, S.; Le, N. D. B.; Mout, R.; Saha, K.; Tonga, G. Y.; Bain, R. E. S.; Miranda, O. R.; Rotello, C. M.; Rotello, V. M. *Nat. Nanotechnol.* **2015**, *10*, 65−69.
(34) Hizir, M. S.; Robertson, N. M.; Balcioglu, M.; Alp, E.; Rana, M.; Yigit, M. V. *Chem. Sci.* **2017**, *8*, 5735−5745.
(35) Chen, W.; Li, Q.; Zheng, W.; Hu, F.; Zhang, G.; Wang, Z.; Zhang, D.; Jiang, X. *Angew. Chem., Int. Ed.* **2014**, *53*, 13734−13739.
(36) Han, J.; Cheng, H.; Wang, B.; Braun, M. S.; Fan, X.; Bender, M.; Huang, W.; Domhan, C.; Mier, W.; Lindner, T.; Seehafer, K.; Wink, M.; Bunz, U. H. F. *Angew. Chem., Int. Ed.* **2017**, *56*, 15246−15251.
(37) Qin, L.; Wang, X.; Liu, Y.; Wei, H. *Anal. Chem.* **2018**, *90*, 9983.
(38) Wu, G.-W.; He, S.-B.; Peng, H.-P.; Deng, H.-H.; Liu, A.-L.; Lin, X.-H.; Xia, X.-H.; Chen, W. *Anal. Chem.* **2014**, *86*, 10955−10960.
(39) Nguyen, T. D.; Scherer, G. G.; Xu, Z. J. *Electrocatalysis* **2016**, *7*, 420−427.
(40) Niu, L.-Y.; Chen, Y.-Z.; Zheng, H.-R.; Wu, L.-Z.; Tung, C.-H.; Yang, Q.-Z. *Chem. Soc. Rev.* **2015**, *44*, 6143−6160.
(41) Yin, J.; Kwon, Y.; Kim, D.; Lee, D.; Kim, G.; Hu, Y.; Ryu, J.-H.; Yoon, J. *J. Am. Chem. Soc.* **2014**, *136*, 5351−5358.
(42) Sun, Y.; Wang, J.; Li, W.; Zhang, J.; Zhang, Y.; Fu, Y. *Biosens. Bioelectron.* **2015**, *74*, 1038−1046.

DOI: 10.1021/acs.analchem.8b03374
Anal. Chem. 2018, 90, 11696−11702